CHAPTER 6

CFD STUDY ON MODIFIED MINICHANNEL HEAT SINK

The modification in surfaces by means of waviness, ribs, dimples, fins, etc. and use of turbulators to create flow disturbance come under passive techniques of heat transfer augmentation. In the present study, different types of ribs have been employed for flow disturbance in minichannel heat sink. Four different types of ribs and hybrid nanofluids have been considered in the present numerical investigation. Semi-circular, rectangular, triangular and trapezoidal ribs are taken for the study. The DI water, Al_2O_3+TiO_2/Di water and Al_2O_3+Cu/DI water hybrid nanofluids has been employed here as working fluids.

6.1 Methodology

The multiphase mixture model is used for the numerical simulation for the modified minichannel heat sink. Governing equations and other details about the mixture model have been provided in section 5.1 of chapter 5.

6.2 Geometry and meshing

In the present study, the schematic of minichannel heat sink is shown in Fig. 6.1. Dimensions are also presented in Fig. 6.1. The length, width and height of the minichannel heat sink are 30 mm, 20 mm and 10 mm, respectively. 9 channels have been developed on aluminium heat sink. The acrylic plate is used to cover the minichannel heat sink. Dimensions of rectangular-shaped minichannel are length = 30 mm, width = 1 mm and depth = 3 mm. Three elements in the system are acrylic material, aluminium material and working fluid. The computational domain is shown in

Fig. 6.1 by the dotted line. It consists of a single full-length channel with periodic boundaries. Symmetric boundary conditions have been applied to the lateral surface of the computational domain. For meshing, the quadrilateral mesh has been applied to all the zones.

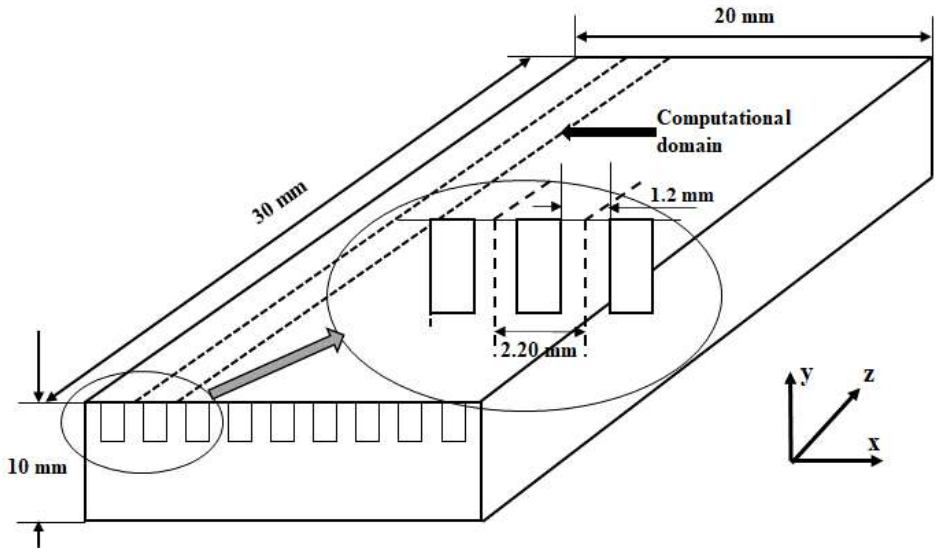

Fig. 6.1 Schematic of minichannel heat sink

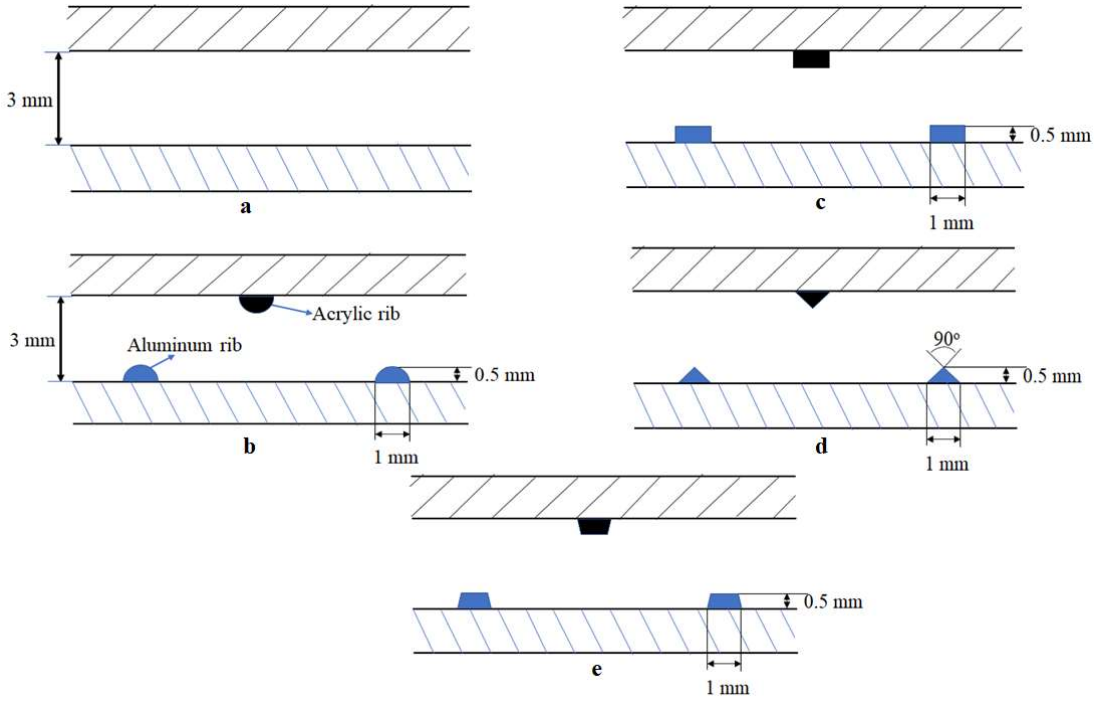

Fig. 6.2 Configuration of channel (a) Plane channel (b) semi-circular ribs (c) rectangular ribs (d) triangular ribs and (e) trapezoidal ribs

The configuration of channels is presented in Fig. 6.2. Four types of ribs are considered in the present numerical investigation. These are semi-circular ribs, rectangular ribs, triangular ribs and trapezoidal ribs. The acrylic plate is used to cover the channel from the upper side. Ribs are provided bottom and upper side of the channel. Upper side ribs are made of acrylic material and attached to the acrylic plate. Lower side ribs are made of aluminium and attached to aluminium material (channel made of from the same material). Height, width and length of ribs are 0.5 mm, 1 mm and 1 mm, respectively. Width of ribs is similar to the width of the channel in each case (i.e., 1 mm). The center of the first acrylic rib is 7.5 mm from the inlet and other ribs are placed with a pitch of 5 mm having 4 acrylic ribs in each case. The center of the first aluminium rib is 5 mm downstream from the inlet in each case and other ribs are placed with a pitch of 5 mm having 5 aluminium ribs in each channel in a decorated pattern. In Fig. 6.3, the computational domain with boundary condition and ribs position has been presented in 2D. The length, height and width of the computational domain are 30 mm, 10 mm and 2.2 mm, respectively. In Fig. 6.3, dashes line at side walls and upper side shows the insulation for no heat losses to the surrounding. Assumptions and other boundary conditions are provided in section 5.1.3 of chapter 5. Table 6.1 presents the ribbed channels with their enlargement factors. Here enlargement factor is defined as the ratio of the surface area of the ribbed channel and surface are of the plane channel (without ribs). The rectangular ribbed channel has the highest enlargement factor as 1.0289. The ascending order of enlargement factor is Triangular < Semi-circular < Trapezoidal < Rectangular.

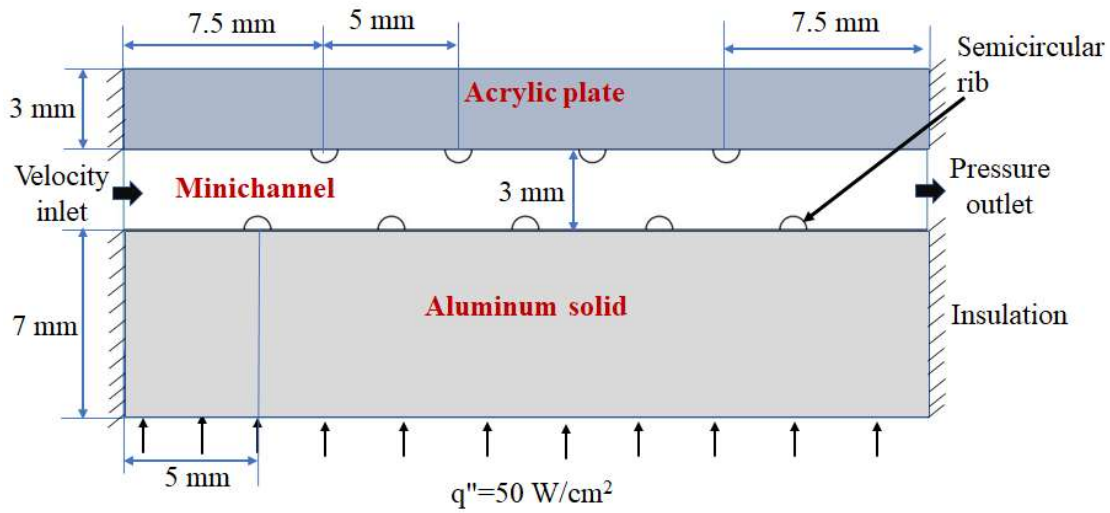

Fig. 6.3 Computational domain with boundary conditions and ribs positions in 2D (width is not showing here)

Table 6.1 Types of the ribbed channel with their enlargement factor

Type of ribbed channel	Enlargement factor
Semi-circular	1.0242
Rectangular	1.0289
Triangular	1.0211
Trapezoidal	1.0243

6.3 Numerical procedure

The governing equations for the multiphase mixture model are provided in section 5.1.1 of the previous chapter (chapter 5). ANSYS 18 fluent software has been used to solve the governing equations. The finite volume method and first-order upwind scheme have been employed for the discretization of governing equations. For solving velocity-pressure coupled equations, the SIMPLE algorithm has been used. User-defined function (UDF) for the required thermophysical properties of hybrid nanofluid has been prepared based on the correlation provided in the previous chapter 5. These

UDFs are inserted in the fluent software and simulation has been performed. The residual was equivalent to 10-6 for each equation in order to manage the numerical error and ensure iteration numbers.

6.4 Grid independence test and validation

In the study, to ensure the independency of mesh size, a grid independence test is conducted. Optimum grid number has been calculated by its effect on heat transfer coefficient and pressure drop. The result for plan channel (without ribs) has been provided in section 5.4 of chapter 5. As discussed, the very fine grid is selected for simulation. The numerical result for Al_2O_3/DI water nanofluid at an inlet temperature of 30°C is validated with the outcome of performed experiments. 22.57% and 13.21% deviations in the Nusselt number and friction factor have been observed from the experimental result, respectively. Other information has been provided in section 5.5 of chapter 5.

6.5 Results and discussion

In this section, heat transfer and pressure drop characteristics of the different combinations of ribs and hybrid nanofluids are discussed. Table 6.2 compares the combined effect of different ribs and working fluids on various parameters as heat transfer coefficient, Nusselt number, pressure drop, friction factor and comparison factor ($h/\Delta p$) at a flow rate of 0.3 lpm. Heat transfer coefficient and Nusselt are highest for Al_2O_3+Cu hybrid nanofluid in all plane/ribbed channels. Also, Al_2O_3+Cu hybrid nanofluid has the highest penalty of pressure drop in all channels. The maximum value of the heat transfer coefficient yielded by a semi-circular ribbed channel with Al_2O_3+Cu hybrid nanofluid. The plane channel (without ribs) has a maximum comparison factor

(h/Δp) as compared to all other ribbed channels with and without hybrid nanofluids. This is because the pressure drop is increasing faster than the heat transfer coefficient in considered ribbed channels.

Table 6.2 Comparison of different ribs and working fluids based on various parameters at a flow rate of 0.3 lpm

Types of channel	**Working fluids**	**Parameters**				
		h (W/m^2K)	**Nu**	**Δp (Pa)**	**f**	**J (m/s.K)**
Plane channel	**DI water**	3156.1	7.64	112.23	0.33	28.18
	Al_2O_3+TiO_2	3404.3	8.14	129.42	0.38	26.39
	Al_2O_3+Cu	4067.9	9.49	144.16	0.42	28.29
Semi-circular ribbed channel	**DI water**	3207.8	7.76	145.07	0.42	22.12
	Al_2O_3+TiO_2	4118.9	9.85	173.01	0.50	23.81
	Al_2O_3+Cu	4789.1	11.17	188.03	0.55	25.47
Rectangular ribbed channel	**DI water**	3155.3	7.63	155.58	0.45	20.28
	Al_2O_3+TiO_2	3915.4	9.37	183.70	0.54	21.31
	Al_2O_3+Cu	4560.0	10.64	198.79	0.58	22.94
Triangular ribbed channel	**DI water**	3348.0	8.10	134.47	0.39	24.90
	Al_2O_3+TiO_2	4053.4	9.70	181.96	0.53	22.28
	Al_2O_3+Cu	4718.7	11.00	197.06	0.58	23.94
Trapezoidal ribbed channel	**DI water**	3213.0	7.77	151.59	0.44	21.19
	Al_2O_3+TiO_2	3914.8	9.37	176.30	0.51	22.20
	Al_2O_3+Cu	4563.4	10.65	191.39	0.56	23.84

In all the graphs, AT and AC are abbreviations for Al_2O_3+TiO_2 and Al_2O_3+Cu dispersed hybrid nanofluids, respectively. Results of the plane channel (i.e., without ribs) are shown by solid lines, whereas for all other ribbed channels, dotted lines are used in the figures. The heat transfer coefficient is rising with the flow rate, as depicted in Fig. 6.4. It can be concluded from Fig. 6.4 that the Al_2O_3+TiO_2 is less effective as compared to Al_2O_3+Cu hybrid nanofluid in term of heat transfer coefficient because for each rib, Al_2O_3+TiO_2 dispersed hybrid nanofluid yield less heat transfer coefficient. Semi-circular ribs with Al_2O_3+Cu hybrid nanofluid yield the maximum value for the heat transfer coefficient due to uniform streamlines in semi-circular ribs and higher thermal conductivity of copper nanoparticles. This is further discussed in the present chapter.

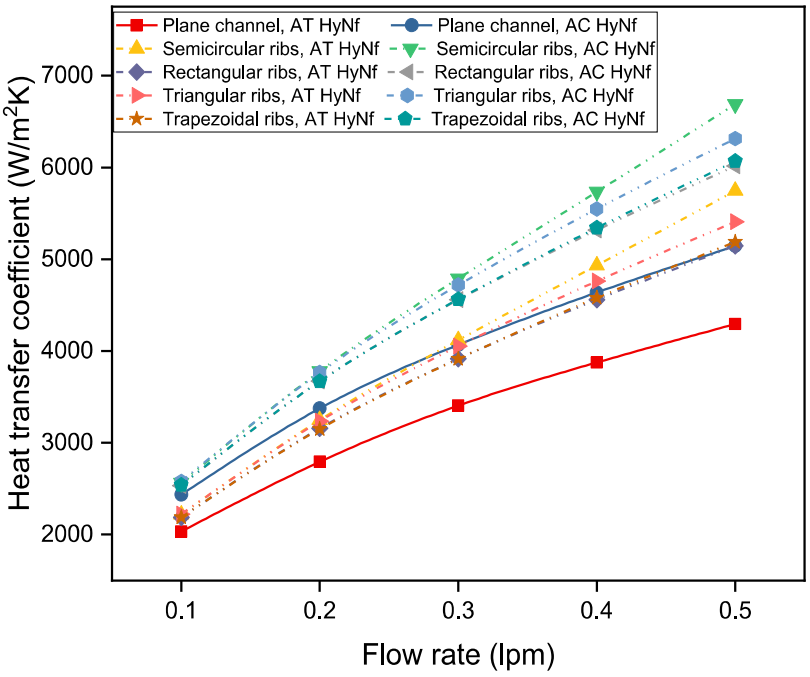

Fig. 6.4 Changing of heat transfer coefficient with flow rate

The variation of Nusselt number with Reynolds number for all configured ribs channel is depicted in Fig. 6.5. Nusselt number is increasing with the rise in flow rate. It can be seen that all configured ribs channels have a high Nusselt number with

Al_2O_3+Cu over Al_2O_3+TiO_2 dispersed hybrid nanofluid. Channel with semi-circular ribs yields maximum Nusselt number. This is due to in other ribs system, the working fluid stagnate between the ribs due to low velocity and create thermal resistance. But in the circular ribs system, the fluid flow on the circular ribs uniformly. For a particular hybrid nanofluid, rectangular ribs yield minimum Nusselt number and semi-circular ribs demonstrate maximum Nusselt number. As in Table 6.1, the enlargement factor is highest for rectangular, followed by trapezoidal, semi-circular and triangular ribbed channels. But the role of the surface area is not significant in the present problem due to the domination of thermal resistance creates by stagnation of fluid between ribs in the rectangular and trapezoidal ribbed channels.

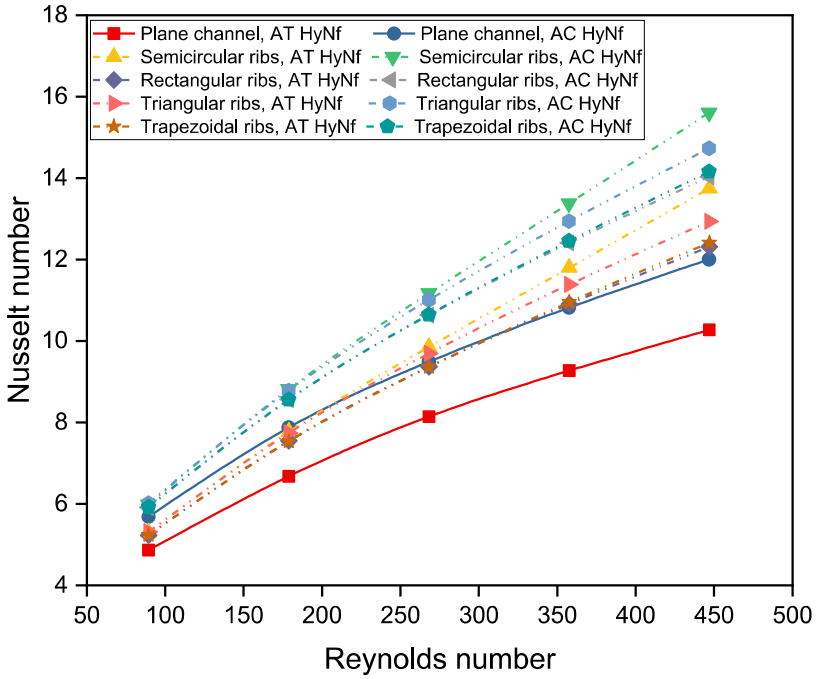

Fig. 6.5 Changing of Nusselt number with Reynolds number

The ratio of Nusselt number with hybrid nanofluid and with water is discussed to analyze the effect of hybrid nanofluid over DI water (base fluid). The ratio of Nu_{HyNf}/Nu_{Water} with Reynolds number is presented in Fig. 6.6. It can be seen that for all

the cases, Nu_{HyNf}/Nu_{Water} is more than 1. It means that hybrid nanofluids yield more Nusselt number as compared to DI water. For semi-circular ribs, the ratio Nu_{HyNf}/Nu_{Water} is high as compared to all other configured rib channels. Al_2O_3+Cu dispersed hybrid nanofluid show the same pattern as Al_2O_3+ TiO_2 hybrid nanofluid, but in each case, Al_2O_3+Cu yields high Nu_{HyNf}/Nu_{Water} ratio because of the high thermal conductivity of copper nanoparticles. Semi-circular ribs with Al_2O_3+Cu and Al_2O_3+ TiO_2 dispersed hybrid nanofluids show that Nu_{HyNf}/Nu_{Water} ratio is increasing within the studied range of Reynolds number and all other ribbed channels present increasing-decreasing trends of Nu_{HyNf}/Nu_{Water}. This is because at low Reynolds number, properties are dominating and at high Reynolds number, flow is dominating on heat transfer.

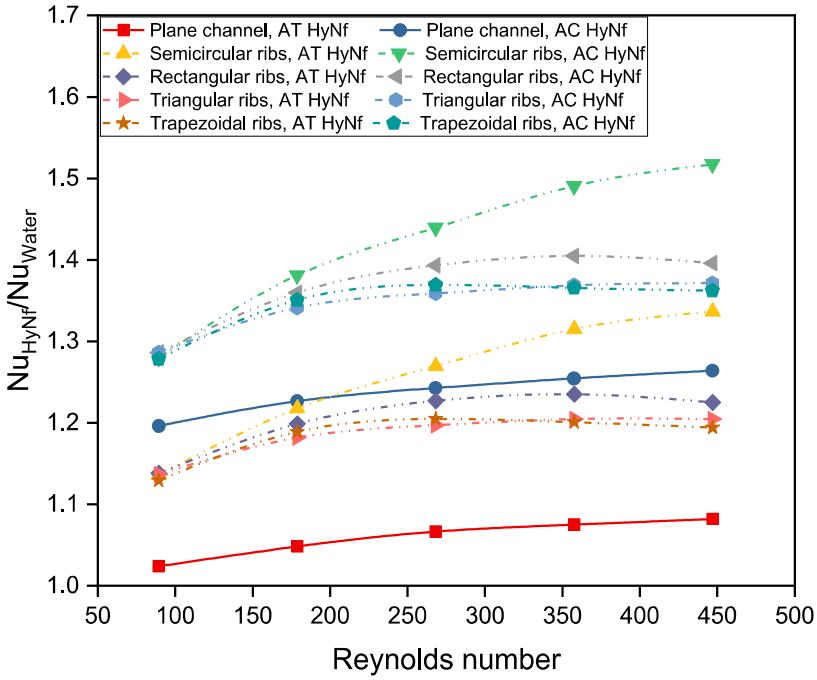

Fig. 6.6 Effect of hybrid nanofluid over water on Nusselt number

Fig. 6.7 depicts the pressure drop variation with the volume flow rate for all configured ribbed channels. It can be seen from Fig. 6.7 that the for same flow rate, pressure drop in the ribbed channel are far from the plane channel (i.e., without ribs). This is due to the hindrance in fluid flow due to ribs. As the flow rate rises, the

deviation of pressure drop in the ribbed channel is higher from the plane channel and has a maximum deviation at 0.5 lpm in the studied range of flow rate. This is due to the dominance of mass velocity over the viscosity at the high flow rate (Reynolds number). There is sufficient difference in pressure drop for rectangular ribbed channel and semi-circular ribbed channel. Maximum pressure drop is observed for the rectangular ribbed channel with Al_2O_3+Cu dispersed hybrid nanofluid and semi-circular ribbed channel with Al_2O_3+TiO_2 dispersed hybrid nanofluid demonstrate the minimum pressure drop (This is due to streamline flow in case of semi-circular ribbed channel) within the studied configurations of the ribbed channel. For a particular hybrid nanofluid, the pressure drop in ascending order is shown for semi-circular ribs, trapezoidal ribs, triangular ribs and rectangular ribs.

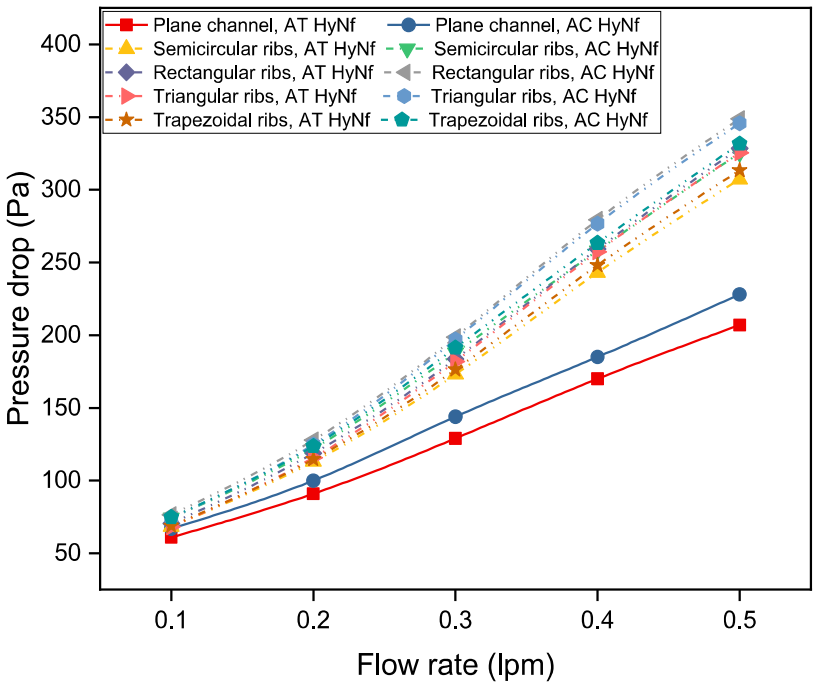

Fig. 6.7 Changing of pressure drop with the flow rate

Variation of friction factor with Reynolds number for all configured ribbed channels and the plane channel is presented in Fig. 6.8. As the Reynolds number rises,

the friction factor shows decreasing trends. Rectangular ribs and semi-circular ribs show the maximum and minimum friction factor respectively within studied range of Reynolds number for a particular hybrid nanofluid, but there is no much variation in friction factor for Rectangular ribs and semi-circular ribs. The ratio f_{HyNf}/f_{Water} with Reynolds number is presented in Fig. 6.9 for all configured ribs channel. f_{HyNf}/f_{Water} ratio is more than 1 for all the configured ribbed channels. The trend of f_{HyNf}/f_{Water} ratio is the same for both Al_2O_3+TiO_2 and Al_2O_3+Cu dispersed hybrid nanofluids. f_{HyNf}/f_{Water} ratio has increasing-decreasing-increasing trends for the plane channel as well as all configurations of the ribbed channel. The f_{HyNf}/f_{Water} ratio is maximum for triangular ribs with both hybrid nanofluids. The slop of f_{HyNf}/f_{Water} ratio for triangular ribs is maximum.

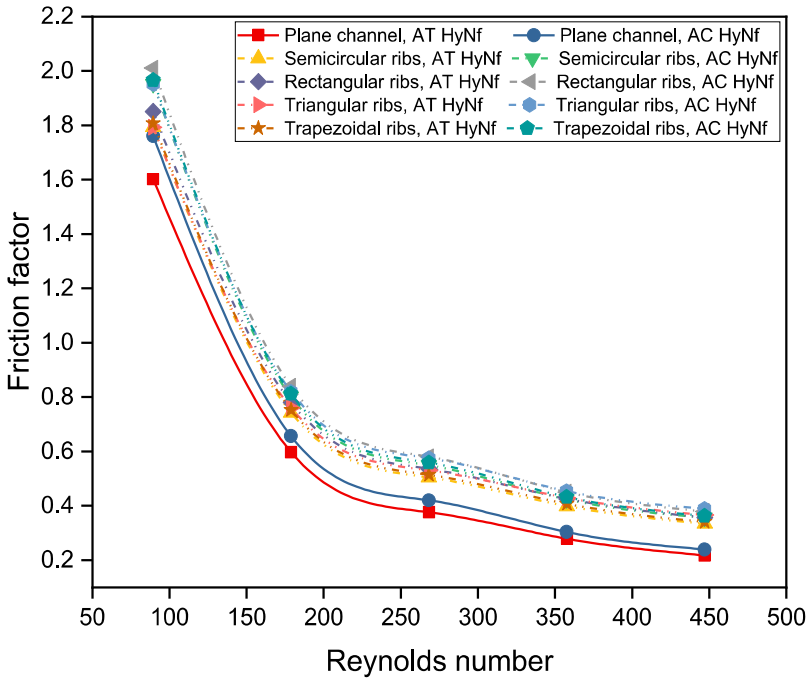

Fig. 6.8 Changing of friction factor with Reynolds number

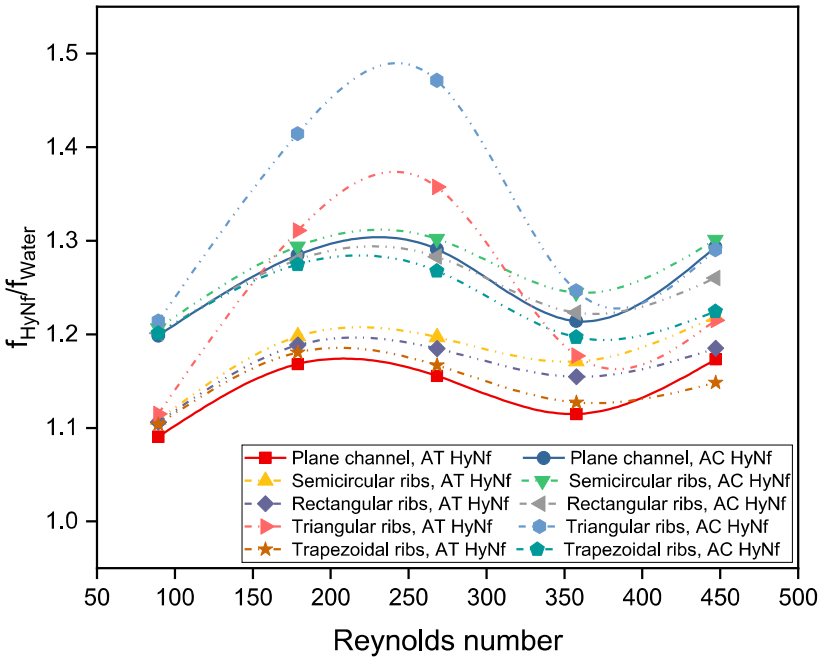

Fig. 6.9 Effect of hybrid nanofluid over water on friction factor

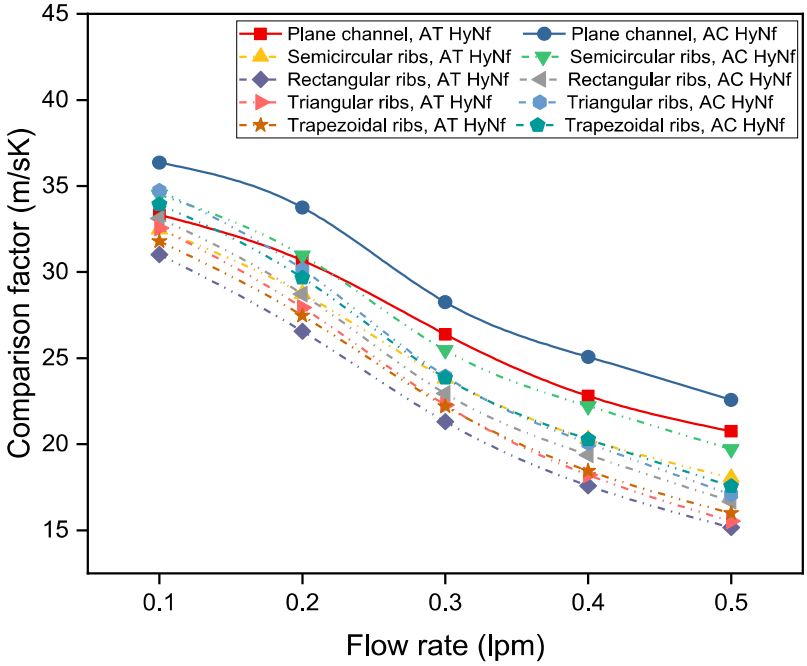

Fig. 6.10 Comparison factor (h/Δp) with flow rate

Fig. 6.10 depicts the variation of Comparison factor (h/Δp) with flow rate for all configurations of the ribbed channel. It can be demonstrated that the h/Δp ratio is maximum for the plane channel as compared to all configured ribbed channels. It

concludes that the pressure drop increases at a faster rate as compared to the heat transfer coefficient in the ribbed channel. The semi-circular ribbed channel presents a maximum h/Δp ratio and the rectangular ribbed channel shows a minimum h/Δp ratio within all configurations of the ribbed channel.

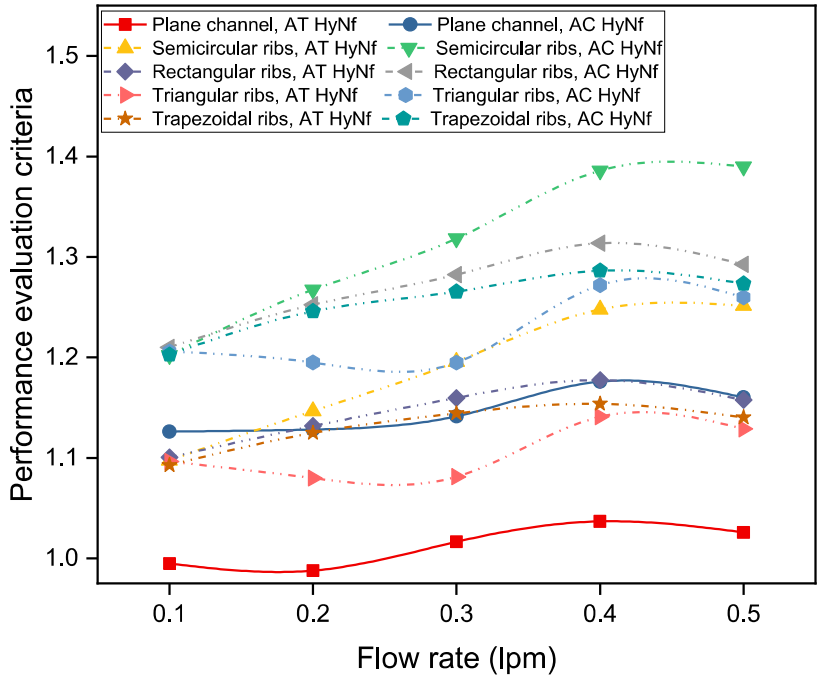

Fig. 6.11 Performance evaluation criteria with flow rate

Performance evaluation criteria (PEC) is the assessment between Nusselt number and friction factor comparing to the hybrid nanofluid as the water (base fluid). Variation of PEC with the flow rate in the range of 0.1-0.5 lpm is demonstrated in Fig. 6.11. It can be indicating that semi-circular ribs show maximum PEC value in comparison to all other combinations of ribs and hybrid nanofluid. In the case of hybrid nanofluids Al_2O_3+Cu is better as compared to Al_2O_3+TiO_2 mixture. PEC value is more than 1 for all the cases except plan channel with Al_2O_3+TiO_2 dispersed hybrid nanofluid at a lower flow rate. The maximum PEC value is observed as about 1.40 for semi-circular ribs at 0.5 lpm.

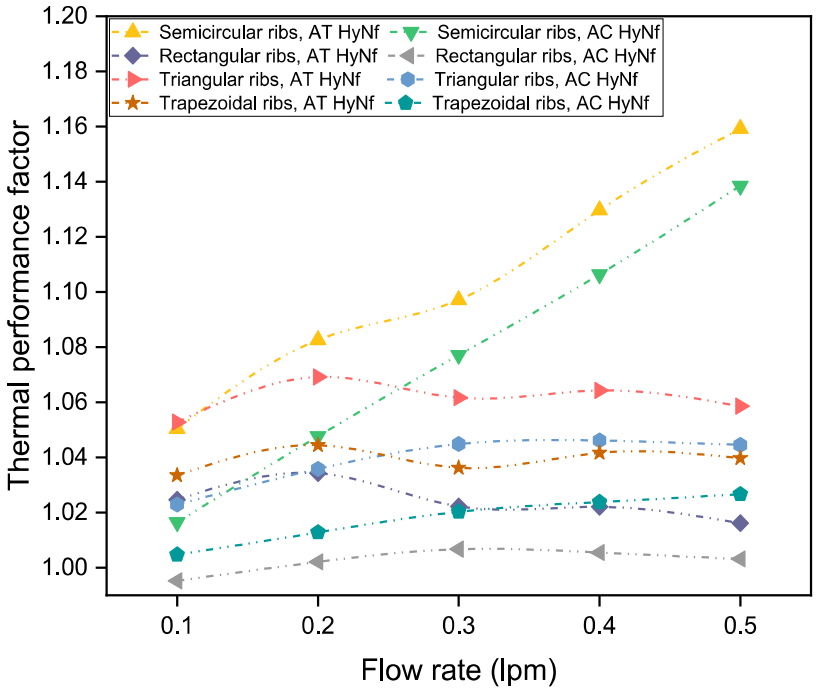

Fig. 6.12 Changing of thermal performance factor with flow rate

Above results show that thermal and hydraulic performances both increase from the interrupting channel using different ribs. Thus, a combined assessment factor is applied to investigate the effect of different ribs. The high thermal performance factor (TPF) is favorable. TPF is the ratio of Nu_r/Nu_{pc} and f_r/f_{pc} and given as follow,

$$TPF = \frac{(Nu_r / Nu_{pc})}{(f_r / f_{pc})^{1/3}} \tag{6.1}$$

Fig. 6.12 show the variation of thermal performance factor with flow rate for all configured ribs channel. The figure demonstrates that the semi-circular ribs with Al_2O_3+TiO_2 dispersed hybrid nanofluid yield maximum thermal performance factor of about 1.6. Only the semi-circular ribbed channel with both hybrid nanofluids shows increasing trends with flow rate. Rectangular ribbed channel with Al_2O_3+Cu has TPF less than 1 which means that friction factor dominates over Nusselt number in this case.

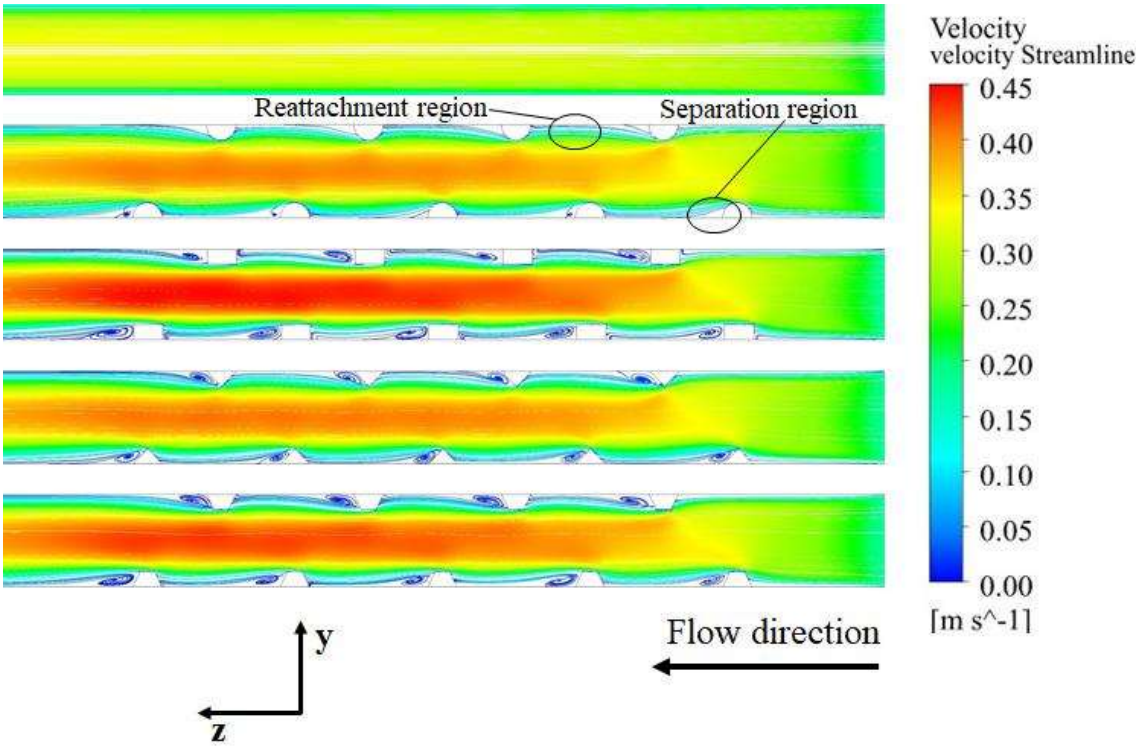

Fig. 6.13 Velocity streamline on the y-z plane for all channels (with and without ribs) with Al_2O_3+Cu/DI water hybrid nanofluid at Re= 268.13 and x/L_x=0.5

Fig. 6.13 presents the velocity streamlines using Al_2O_3+Cu/DI water hybrid nanofluid on the y-z plane for all channels (with and without ribs) at Re= 268.13 and x/L_x=0.5. It demonstrates the effect of ribs on flow behavior. It can be observed that as the fluid reaches over ribs, it gets deflected and move to other walls with more velocity because of reduction in area. Here the concept of separation region and reattachment region is discussed. Separation and reattachment regions are shown in the semi-circular ribbed channel. As the working fluid passes through the ribs, the fluid velocity downstream to ribs decreases and flow separation is observed. The working fluid does not stagnant between the semi-circular ribs due to uniform streamlined in semi-circular ribs. But in the rectangular, trapezoidal and triangular ribbed channels, the fluid gets stuck and stagnant between two consecutive ribs, which causes for the rise in thermal

resistance. This is the reason for the high heat transfer coefficient and low pressure drop in semi-circular ribbed channel.

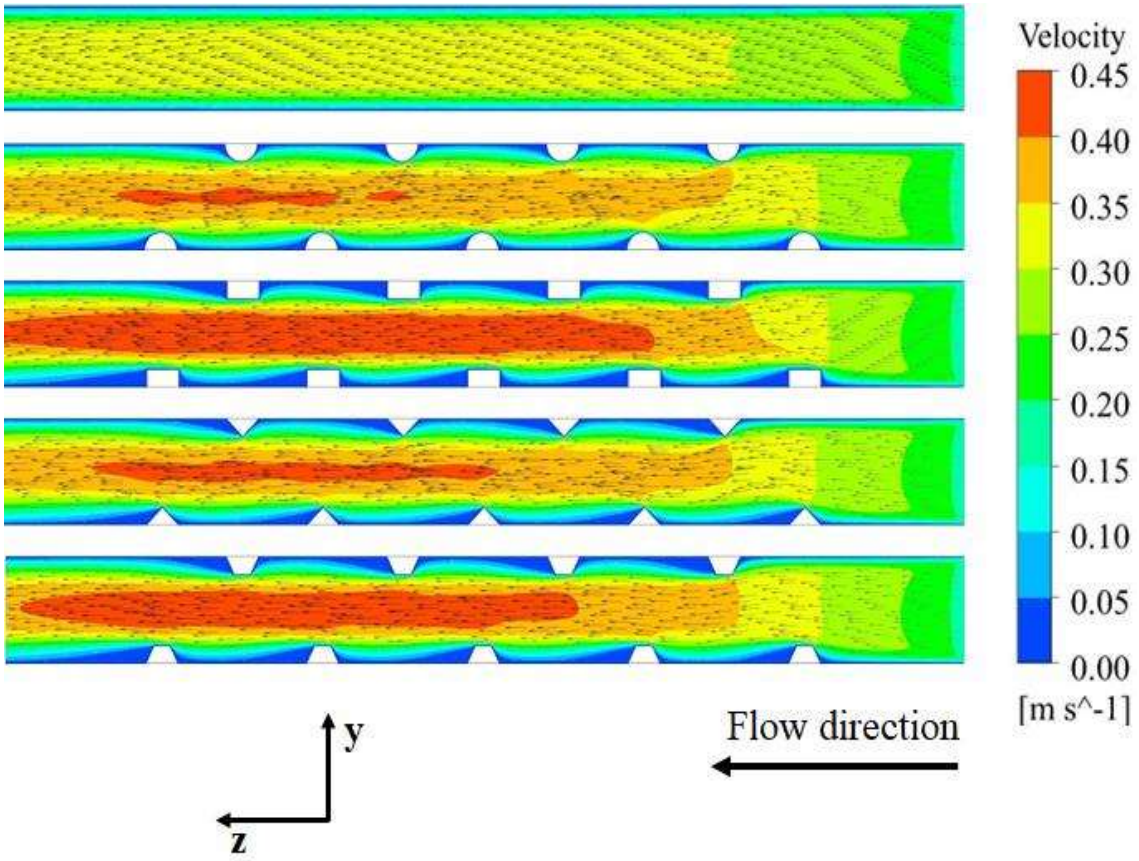

Fig. 6.14 Velocity contour and vectors on the y-z plane for all channels (with and without ribs) with Al_2O_3+Cu/DI water hybrid nanofluid at Re= 268.13 and x/L_x=0.5

Velocity distribution and vectors using Al_2O_3+Cu/DI water hybrid nanofluid on the y-z plane for all channels (with and without ribs) at Re= 268.13 and x/L_x=0.5 is presented in Fig. 6.14. It can be observed that the plane channel has a big region for low speed of working fluid, which is not favorable for heat transfer improvement. The rectangular and trapezoidal ribbed channels have higher velocity region as compared to others. This is the reason for high pressure drop as compared to other ribbed channels. From the vector, it can be seen that the fluid disturbed by the ribs and move to center of

the channel. This center pressure pushes the fluid to other walls and mainstream mixed with the hot fluid near the wall. But in Rectangular and trapezoidal ribbed channel stagnant of fluid between two ribs occurred, the reason for high thermal resistance leads to low heat transfer rate.

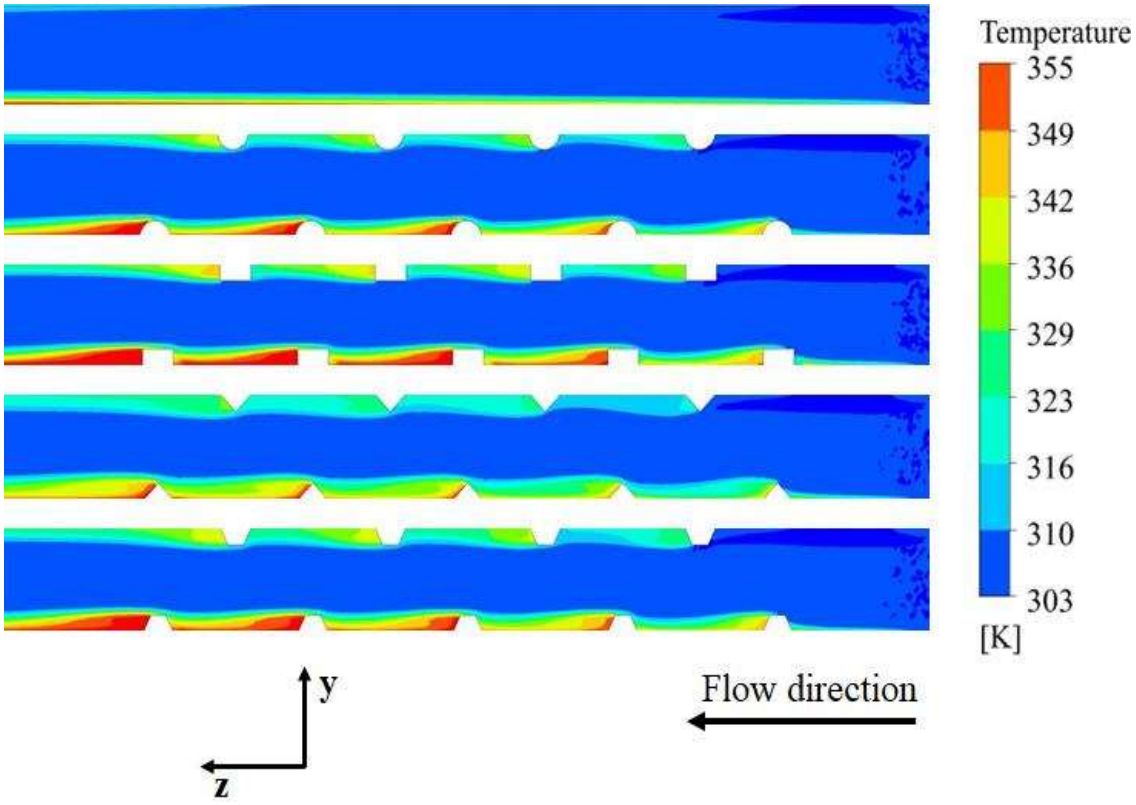

Fig. 6.15 Temperature contour on the y-z plane for all channels (with and without ribs) with DI water at Re= 277.08 and x/L_x=0.5

Temperature contours using DI water and Al_2O_3+Cu hybrid nanofluid on the y-z plane for all channels at Re = 277.08 (correspond to DI water) and 268.13 (correspond to Al_2O_3+Cu hybrid nanofluid) and x/L_x=0.5 are illustrated in Fig. 6.15 and 6.16, respectively. The low temperature zone is at the channel center and high-temperature zone is adjacent to the channel wall. It is noticed from both the figures that the

improvement in temperature uniformity occurs and temperature decreases with the hybrid nanofluids as compared to DI water. Also, the highest temperature region becomes smaller by using hybrid nanofluid. It can be seen that for the rectangular and trapezoidal ribbed channels, the heat transfer rate is lower between ribs because of the stagnant fluid creates the thermal resistance. It can also be observed that rectangular and trapezoidal ribbed channels have more heated fluid in between the upper side ribs as compared to the triangular and circular ribbed channels. Acrylic ribs on the upper side to channel are provided to only create better turbulence to flowing fluid, which leads to better mixing of fluid near the wall.

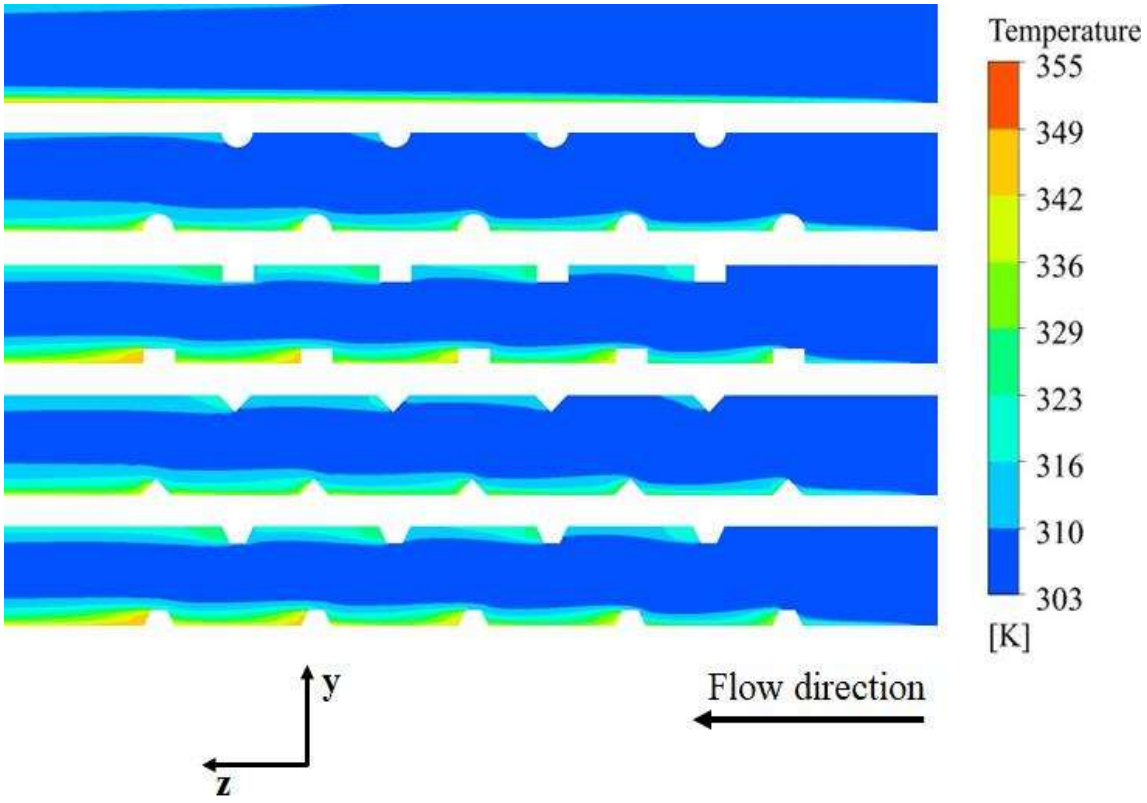

Fig. 6.16 Temperature contour on the y-z plane for all channels (with and without ribs) with Al_2O_3+Cu/DI water hybrid nanofluid at Re= 268.13 and x/L_x=0.5

6.6 Effect of pitch of ribs

The effect of pitch of ribs may be an interesting study. It is directly related to the number of ribs. It is presented in the literature that the Nusselt number and friction factor ratio (Nu_r/Nu_{pc} and f_r/f_{pc}) both increase with rise in number of ribs **(Akbari et al., 2015, Ghale et al., 2015)**. It concludes that thermal performance improves but on the penalty of hydraulic performance loss. **Ghale et al., 2015** studied a rectangular microchannel with different numbers (3, 5 and 9) of rectangular shaped ribs at bottom wall of channel. They presented that hydraulic performance is optimized for 5 number of ribs based on hydraulic performance. Thus, the combined effect of thermal performance and hydraulic performance (i.e., hydrothermal performance) may be improved or vice-versa. for better hydrothermal performance, number of ribs has to be optimized.

6.7 Highlights

- Semi-circular rib with Al_2O_3+Cu hybrid nanofluid yields maximum heat transfer coefficient and Nusselt number.
- Al_2O_3+TiO_2 is less effective as compared to Al_2O_3+Cu hybrid nanofluid in terms of heat transfer coefficient and Nusselt number.
- The maximum and minimum pressure drop and friction factor are observed for rectangular ribbed channel and semi-circular ribbed channel, respectively.
- Comparison factor (heat transfer coefficient to pressure drop ratio, $h/\Delta p$) is maximum for the plane channel as compared to all configured ribs channel due to a faster rate of pressure drop penalty as compared to the heat transfer coefficient.
- PEC value is more than 1 for all the cases except plan channel with Al_2O_3+TiO_2 dispersed hybrid nanofluid at a lower flow rate.

- Semi-circular ribbed channel with both Al_2O_3+Cu and Al_2O_3+TiO_2 hybrid nanofluids shows increasing trends of thermal performance factor with flow rate.
- The working fluid gets stuck and stagnant between two consecutive ribs in Rectangular, trapezoidal and triangular ribbed channels, which causes a rise in thermal resistance leads to deteriorating heat transfer performance.